Dry snow parameter retrieval with ground-based single-pass Synthetic Aperture Radar Interferometry

Yang Lei, Xiaolan Xu, *Senior Member, IEEE,* Chad A. Baldi, Jan-willem De Bleser, Simon Yueh, *Fellow, IEEE,* Daniel Esteban-Fernandez, Kelly Elder, Banning Starr, and Paul Siqueira, *Member, IEEE*

***Abstract*—In this paper, we investigate the potential of using single-pass InSAR model-based approaches to retrieve dry snow parameters. Two InSAR scattering models of dry snow are considered: the dense-medium RVoG model and the simple variant of Full Penetration (FP) model. A Quasi-Crystalline Approximation (QCA) based extinction analysis confirms the negligible extinction dependence of the InSAR observables at L/C/X-band for fresh dry snow. The FP models the low-frequency (L/C/X-band) InSAR phase as a single constraint of snow depth and density, which can be supplemented by an extra observation (e.g. InSAR coherence or in-situ depth/density). The single-pass InSAR models and inversion approaches were validated using X-band InSAR data collected from a tower-based three-frequency (X/Ku-low/Ku-high) fully polarimetric TomoSAR system, where a multi-frequency polarimetric InSAR analysis and ground-to-volume ratio-based snow condition analysis were conducted. We also analyzed the sensitivity and error propagation of the single-pass InSAR phase and coherence in measuring dry snow depth/density. It was found that the X-band HH-pol FP-modeled single-pass InSAR phase along with RVoG-modeled coherence or in-situ depth is capable of measuring Snow Water Equivalent (SWE) with a 23-26 mm uncertainty (13-15%) and a 20-26 mm bias (12-15%) for dry snow SWE of 0.2 m, and with an optimal perpendicular baseline on the order of a tenth of the snow depth (0.8 m) at our test site. This single-pass InSAR approach with FP model is potentially useful and thus needs further investigation for large-scale dry snow retrieval with a wide range of snow conditions using ground-based/airborne/spaceborne low-frequency (L/C/X-band) InSAR observations.**

***Index Terms*—single-pass, InSAR, phase, coherence, RVoG, dense medium, scattering model, Quasi-Crystalline Approximation (QCA), dry snow, depth, density, Snow Water Equivalent (SWE), ground-based, spaceborne, airborne**

I. Introduction

The research was carried out in part at the Jet Propulsion Laboratory, California Institute of Technology, under a contract with the National Aeronautics and Space Administration. U.S. Government sponsorship acknowledged.

Yang Lei is with Division of Geological and Planetary Sciences, California Institute of Technology, Pasadena, CA, 91125 USA (e-mail: ylei@caltech.edu).

Xiaolan Xu, Jan-willem De Bleser, Simon Yueh and Daniel Esteban-Fernandez are with Jet Propulsion Laboratory, California Institute of Technology, Pasadena, CA, 91109 USA (email: xiaolan.xu@jpl.nasa.gov, jan-willem.de.bleser@jpl.nasa.gov, Simon.H.Yueh@jpl.nasa.gov, Daniel.Esteban-Fernandez@jpl.nasa.gov).

Chad A. Baldi is with Baldi Designs, Inc. (email: chad@baldidesigns.com).

Kelly Elder and Banning Starr are with United States Forest Service, United States Department of Agriculture (USDA), Fort Collins, CO 80526 USA (email: kelly.j.elder@usda.gov, banning.j.starr@usda.gov).

Paul Siqueira is with the Department of Electrical and Computer Engineering, University of Massachusetts at Amherst, Amherst, MA 01003 USA (email: siqueira@umass.edu).

SNOW parameters such as snow water equivalent (SWE), snow density, depth and grain size, are important input variables for understanding and modeling the hydrological cycle, as well as validating the climate change models [1], [2]. This information is also useful for water resource management as well as the forecast of snow weather events such as snowmelt runoff and flooding [3]. Many types of microwave sensors and remote sensing methods have been proposed to retrieve such information [4], including passive radiometer, active scatterometer and Synthetic Aperture Radar (SAR). Among these, spaceborne SAR platforms have the vantage point potential for observing large snow covered regions (typically high topographic relief and polar regions) with complete and dense coverage both spatially and temporally, as well as day/night and all weather observing capability [5].

Furthermore, SAR Interferometry (InSAR) and/or Polarimetric InSAR (PolInSAR) have proven to be very successful in measuring the ground surface elevation along with its changes as well as the depth of volume surface cover (e.g. forest canopy) [6], [7]. Since InSAR with a single SAR platform repeating its orbit or pass (termed "repeat-pass") is mostly sensitive to ground surface changes at sub-wavelength scale, it has been successfully applied to retrieve snow parameters including SWE [8]–[14]. This repeat-pass approach assumes that the radar signal can fully penetrate the snowpack at low frequencies (e.g. L/C-band), and thus the difference of snow-on/off signal path delay can be correlated to snow depth and density, the product of which gives SWE. Without a snow-off dataset but using multiple acquisitions, this repeat-pass approach is further adapted to retrieve the SWE time-series variation, i.e. relative changes only. To determine the absolute amount of SWE, ground control points at a single epoch must be used [9].

The repeat-pass InSAR approach is prone to error due to the temporal decorrelation of the snow cover, e.g. due to snow accumulation, melting, storm, wind, temperature, all of which can affect the scatterers's position, geometry and scattering properties (dielectric content) in the snow cover. The longer temporal baseline, the more likely the physical changes experienced by the ground targets occur thus leading to temporal decorrelation. For spaceborne SAR missions with a repeat cycle of a few days (e.g. ESA's Sentinel-1) to tens of days (e.g. JAXA's ALOS), the temporal decorrelation could overwhelm the InSAR retrievals depending on the type and intensity of snow weather events. Besides temporal decorrelation, this approach is also impacted by atmospheric delay effects (e.g. ionosphere, troposphere) that further delay the

phase path length of the SAR signal.

Another type of InSAR (termed "single-pass") exploits two antennas or platforms so that the two SAR acquisitions can be collected simultaneously (e.g. NASA's SRTM mission) or near-simultaneously with seconds to minutes temporal baseline (e.g. DLR's TanDEM-X mission). Rather than repeat-pass InSAR, the single-pass InSAR approach uses the triangulation of the two SAR phase path lengths from two onboard antennas to accurately determine the elevation of the ground surface target and/or the equivalent scattering center in a volume surface cover (e.g. forest, snow) [6]. Although the measurement accuracy cannot be at sub-wavelength scale, single-pass InSAR is neither subjected to temporal decorrelation errors nor atmospheric delay effects, because of the synchronization, or short time lag, between the two acquisitions. Without inversion using an InSAR scattering model, the single-pass InSAR-derived scattering phase center (e.g. Digital Elevation Model; DEM) was directly used to indicate wet snow depth due to the dominant top surface scattering [15], and used to correct for the elevation bias due to penetration over ice sheets [16]. For dry snow, however, combined surface/volume scattering exists and few studies have examined the potential of the single-pass InSAR approach through inversion of a physical InSAR scattering model.

In this paper, we investigate the potential of using single-pass InSAR to retrieve dry snow parameters by inverting snow InSAR scattering models. In Section II, we introduce the dense-medium Random Volume over Ground (RVoG) model as well as the simplified Full Penetration (FP) model that can be considered the single-pass variant of the above repeat-pass InSAR approach. In Section III, we demonstrate the validation results by using a tower-based TomoSAR system which also has single-pass InSAR capability. A Polarimetric InSAR analysis is first conducted, then followed by a ground-versus-volume scattering power analysis. A performance comparison of snow parameter retrieval from using different InSAR scattering models is also shown, where a sensitivity analysis with error propagation is discussed. Section IV details the conclusion and comparisons of these retrieval methods, and discusses the limitations and future work.

II. Snow InSAR scattering models

A. Dense-medium Random Volume over Ground (RVoG) model

The RVoG model has been originally developed by [7], [17] for retrieving the depth of sparse dielectric medium (such as the height of forest canopy). The simplified single-layer model has been derived to model the observed InSAR complex correlation over half-space dielectric medium (e.g. snow-covered ice sheets) [18], [19]. Then, the original two-layer model was further adapted to a dense dielectric medium (such as snowpack) by incorporating particle grain size, volume fraction (that relates to density) and depth [20], and has also been extended to model a multi-layer medium [21]. In this paper, we focus on the use of the adapted two-layer RVoG model for simplicity without loss of generality.

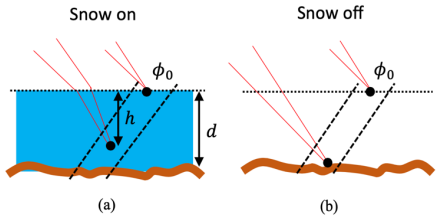

Fig. 1. Illustration of InSAR scattering phase center for (a) snow-on, and (b) snow-off. The InSAR phase at the air-snow interface is denoted as ϕ_0, which is common for both scenarios. The snow-on InSAR phase center is located h below the air-snow interface, and the snow-off phase center is only at the bare ground surface at distance, d, below the air-snow interface.

For a two-layer scenario with a dense random volume (e.g. snowpack) and an underlying ground surface, the apparent single-pass InSAR complex correlation is given by [20]

$$\gamma = \gamma_{\text{SNR}} \cdot \gamma_g \cdot \gamma_v = \gamma_{\text{sys}} \cdot \gamma_v \tag{1}$$

where the γ_{SNR} and γ_g are the InSAR correlation components due to thermal noise and baseline geometry. These are lumped into γ_{sys}, as a systematic InSAR correlation component, which can also assimilate any other systematic decorrelation factors in practice. The remaining term in Eq. 1 is the volumetric correlation, γ_v, which is expressed as [20]

$$\gamma_v = e^{j\phi_g} \frac{\gamma_{\text{vol}} + m}{1 + m} \tag{2}$$

where

$$\gamma_{\text{vol}} = \frac{2k_e/\cos\theta_t}{2k_e/\cos\theta_t + j\kappa_z} \cdot \frac{e^{(2k_e/\cos\theta_t + j\kappa_z)d} - 1}{e^{(2k_e/\cos\theta_t)d} - 1}, \tag{3}$$

$\phi_g = \phi_0 - \kappa_z d$ is the interferometric phase at the ground surface (ϕ_0 is the InSAR phase at the air-snow surface; Fig. 1), m is the Ground-to-Volume power Ratio (GVR), k_e is the extinction coefficient, θ_t is the refraction angle that relates to the incidence angle (θ_i) by Snell's law (i.e., $\sin\theta_i/\sin\theta_t = n$ with n being the refractive index), and the dense-medium interferometric vertical wavenumber κ_z is defined as

$$\kappa_z = \frac{n\cos\theta_i}{\cos\theta_t}\tilde{\kappa_z} \tag{4}$$

with $\tilde{\kappa_z} = \frac{2\pi p B_\perp}{\lambda R \sin\theta_i}$ the free-space wavenumber, $B_\perp$ the perpendicular baseline, λ the free-space wavelength, R the slant range distance, and $p = 1$ ($p = 2$) for the standard-mode (ping-pong-mode) InSAR [6].

From the above model equations, n (that relates to density for dry snow via Looyenga's semi-empirical relationship [22]) and d are needed to calculate SWE, but m and k_e are also unknowns, where k_e implicitly depends on both density and grain size (thus implicitly included in the RVoG model) [20]. Since each InSAR observable (i.e., complex correlation) only has two independent variables, i.e., magnitude and phase, the above RVoG model has to be constrained with two other criteria on m and k_e.

In order to determine the effect of k_e on the InSAR observables and thus make assumptions of its value range, we plot the InSAR coherence as a function of snow depth with various k_e values. This k_e-dependent sensitivity analysis

This article has been accepted for publication in a future issue of this journal, but has not been fully edited. Content may change prior to final publication. Citation information: DOI 10.1109/TGRS.2022.3171269, IEEE Transactions on Geoscience and Remote Sensing

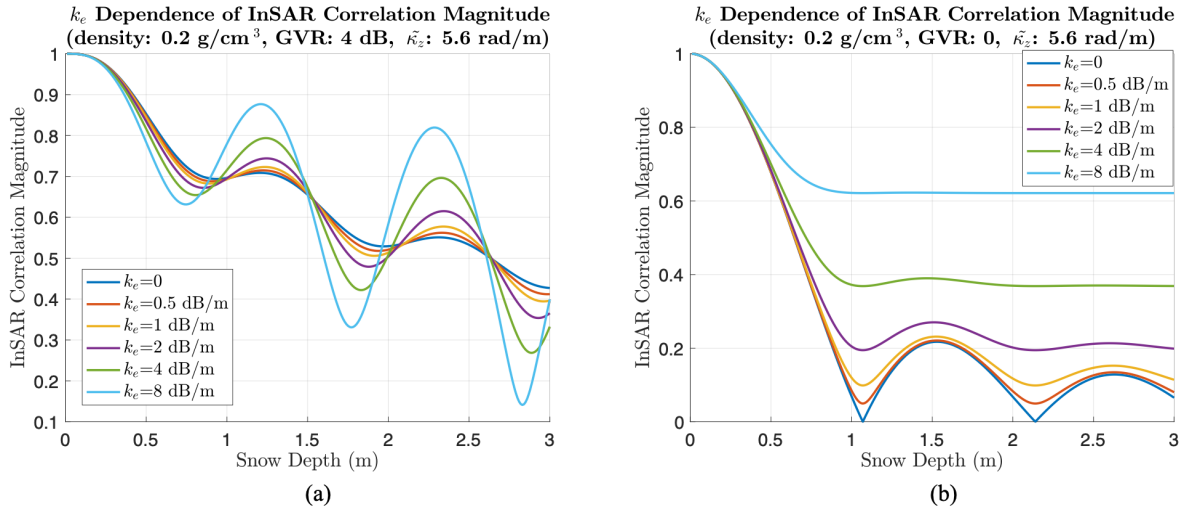

Fig. 2. The k_e dependent sensitivity analysis of the InSAR coherence as a function of snow depth: (a) GVR $m = 4$ dB, and (b) GVR $m = 0$. The snow density is fixed as 0.2 g/cm^3, and the interferometric vertical wavenumber $\tilde{\kappa_z} = 5.6$ rad/m.

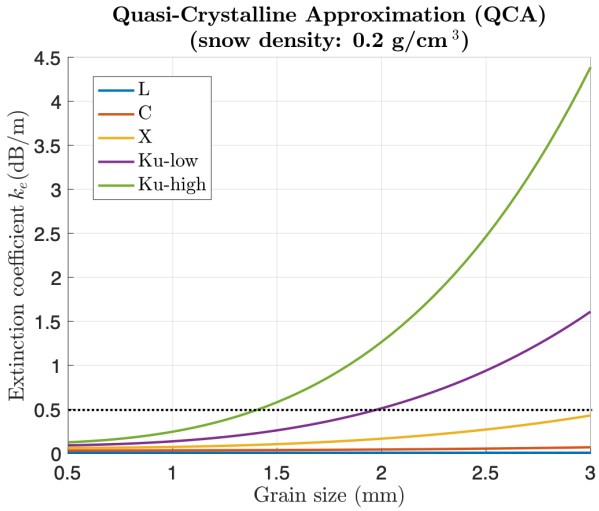

Fig. 3. Quasi-Crystalline Approximation (QCA) dense medium scattering model calculated k_e variation at different frequencies (L-band: 1.25 GHz, C-band: 5.405 GHz, X-band: 9.6 GHz, Ku-low: 13.5 GHz, Ku-high: 17.2 GHz). The threshold of 0.5 dB/m is marked as the black dotted line.

is illustrated in Fig. 2, where Fig. 2a shows the cases when $m = 4$ dB and Fig. 2b shows the cases when $m = 0$. Note the $m = 0$ cases in Fig. 2b are consistent with the sensitivity analysis reported by [23], while the sensitivity curves can change a lot as GVR increases (Fig. 2a). From both Fig. 2a and Fig. 2b, it can be noticed that the sensitivity curve of $k_e = 0.5$ dB/m is almost indistinguishable from that of $k_e = 0$. Therefore, in this paper, we use $k_e = 0.5$ dB/m as a threshold and consider the sensitivity analysis results with $k_e \leq 0.5$ dB/m are equivalent to those of $k_e = 0$.

Next, we investigate the modeled k_e variation at different frequencies. In this paper, we adopt the use of the dense medium scattering model with the Quasi-Crystalline Approximation (QCA) as first introduced to the RVoG InSAR scattering model in [20]. The QCA model-calculated k_e variation is shown in Fig. 3, where the grain size varies from 0.5 mm to 3 mm. The snow density is chosen as 200 kg/m^3, which is both consistent with the observed density at our test site and roughly corresponds to the maximum extinction effect (see [20]). Note for dry snow, the absorption component is considered negligible [16], and thus the extinction is dominated by the scattering part of it, which reaches peak around snow density of 200 kg/m^3. By marking the 0.5 dB/m threshold (determined from the above sensitivity analysis) as the "black" dotted line in Fig. 3, we then notice all of L/C/X-band and part of the Ku-band can be assumed to have zero extinction $k_e = 0$.

More realistic values of k_e need to be used when the absorption is not negligible (wet snow) or the scattering part is significant (snow structure has large aggregate, especially after melt/freeze process), which will be investigated in Section III-D. Unless otherwise noted, in this paper, we assume $k_e = 0$ for fresh dry snow at low frequencies and generate the inversion results under this zero extinction assumption. Letting k_e approach zero turns Eq. 3 to

$$\gamma_{\text{vol}} \underset{k_e \to 0}{=} \frac{e^{j\kappa_z d} - 1}{j\kappa_z d} = e^{j\kappa_z d/2}\text{sinc}(\kappa_z d/2), \tag{5}$$

For calibration of the snow-on InSAR data (as modeled above), we also use the snow-off InSAR observable, which is simply expressed as below,

$$\gamma^{\text{off}} = \gamma_{\text{sys}} e^{j\phi_g^{\text{off}}} \tag{6}$$

where $\phi_g^{\text{off}} = \phi_0 - \tilde{\kappa_z} d$ is the InSAR measured ground phase for the snow-free case (Fig. 1). Hence, by using the snow-off InSAR observable to cancel γ_{sys} and ϕ_0, we have the snow-on/off ratio of InSAR complex correlation given by

$$\begin{aligned} \gamma_{\text{on/off}} &= \frac{\gamma_{\text{sys}}\gamma_v}{\gamma_{\text{sys}} e^{j(\phi_0 - \tilde{\kappa_z} d)}} \\ &= e^{-j(\kappa_z - \tilde{\kappa_z})d} \frac{e^{j\kappa_z d/2}\text{sinc}(\kappa_z d/2) + m}{1 + m} \end{aligned} \tag{7}$$

Therefore, assuming m is given, by substituting Eq. 4, both unknowns of n (or density) and depth d can be inverted

This article has been accepted for publication in a future issue of this journal, but has not been fully edited. Content may change prior to final publication. Citation information: DOI 10.1109/TGRS.2022.3171269, IEEE Transactions on Geoscience and Remote Sensing

from this snow-on/off single-pass InSAR complex correlation ratio. In Section III, we show the estimates of m based on SAR tomography; however, this InSAR approach does not necessarily rely on tomography.

B. Full Penetration (FP) model

Even with some extra assumptions and/or measurements, the above RVoG model is still cumbersome in practical use. In this section we investigate another simplified model, which can be considered the single-pass variant of the repeat-pass InSAR approach [8]–[14] by considering dry snow as a transparent refraction layer at low frequencies (L/C/X-band). From Fig. 1, both the snow-on/off scenarios share the same common InSAR phase ϕ_0 at the air-snow interface. The InSAR scattering phase center ϕ_c of the two scenarios can be easily expressed as

$$\phi_c^{\text{on}} = \phi_0 - \kappa_z h \tag{8}$$
$$\phi_c^{\text{off}} = \phi_0 - \tilde{\kappa_z} d, \tag{9}$$

where h denotes the distance between the scattering phase center and the air-snow interface. Therefore, the snow-on/off InSAR phase difference is given by

$$\delta\phi_c = \phi_c^{\text{on}} - \phi_c^{\text{off}} = -(\kappa_z h - \tilde{\kappa_z} d). \tag{10}$$

From Eq. 4, it can be inferred that $\kappa_z > \tilde{\kappa_z}$ for dielectric medium ($n > 1$). Hence, Eq. 10 can be used to interpret the differential snow-on/off InSAR phase as such: when the radar signal can fully penetrate the snow volume (that acts as a transparent refraction layer) with the scattering center on the ground surface (i.e., $h = d$), $\delta\phi_c < 0$ implying there is a phase lag of the snow-on case compared to the snow-off case; however, when the scattering center moves up (i.e., $h < d$), $\delta\phi_c$ will increase and cross zero to eventually become positive (phase lead). Therefore, given the in-situ data of snow density and depth, we can tell the location of the scattering phase center from the differential snow-on/off InSAR phase.

If we know that the radar signal can fully penetrate the snow volume so that ground scattering dominates (e.g. transparent refraction snow layer with $k_e \ll 1$ and $m \gg 1$ at low frequencies of L/C/X-band), the InSAR apparent phase center is expected to be at the underlying snow-ground interface. Hence, substituting $h = d$ into Eq. 10 gives

$$\delta\phi_c = -(\kappa_z - \tilde{\kappa_z}) d. \tag{11}$$

This Full Penetration (FP) model only relates the two unknowns of density and depth to a single InSAR observable (the differential snow-on/off phase). Unfortunately, Eq. 11 cannot be solved like its repeat-pass counterpart [8], [9] via linearization to establish an analytical relationship between SWE and the apparent InSAR phase. Hence, in order to use this model, an extra dimension of measurement has to be incorporated, which will be discussed in Section III.

III. Validation Results

To validate the single-pass InSAR approach by inverting the above two scattering models (RVoG and FP), in this work, we exploit the tower-based TomoSAR system (SRT3; see Fig. 4) developed by Jet Propulsion Laboratory [24], which has three frequencies (X: 9.6 GHz, Ku-low: 13.5 GHz and Ku-high: 17.2 GHz) with full-polarization capability (see Table I).

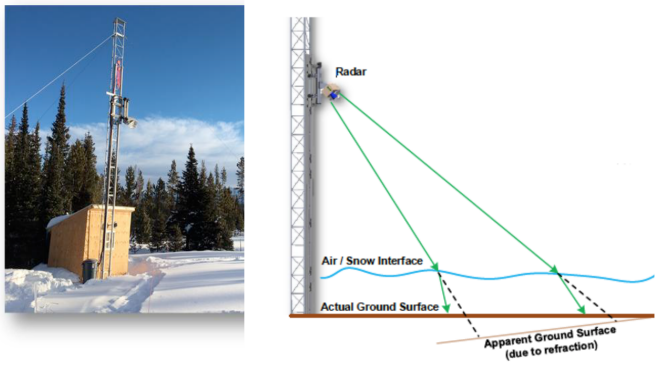

Fig. 4. (Left) SRT3 Deployment at Fraser, CO (Right) Radar setup configuration at 45 degree incidence angle.

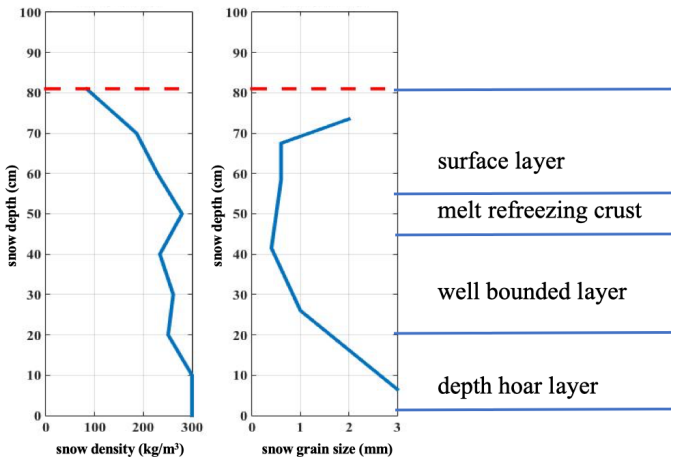

Fig. 5. Snow stratigraphy profiles of the density and grain size collected at the Fraser, CO test site. The data was collected on January 23rd, 2017, which is representative of the whole snow-on period due to the subtle temporal variation of snow parameters [24].

TABLE I
MAJOR SRT3 RADAR PARAMETERS.

	X	Ku-low	Ku-high
Tx Frequency [GHz]	9.35-9.85	13.25-13.75	16.95-17.45
Tx Bandwidth [GHz]	0.5	0.5	0.5
Tx Power [dBm]	0	0	0
Range Resolution [m]	0.3	0.3	0.3
X-pol Isolation [dB]	> 30	> 30	> 30
RCS Sensitivity [dB m^2 m^{-2}]	-55	-55	-55
Horn Beamwidth [deg]	60.3	42.2	35.6
Dish Beamwidth [deg]	5.8	4.1	3.2
X/Y Aperture Length [m]	0.6	0.6	0.6

The radar moved over an aperture of 600 mm $\times$ 600 mm for a full tomographic scan, and we only extract the two lateral tracks of a full scan to form an interferometric pair, where each track has a 600 mm synthetic aperture to focus on the horizontal (ground-range and azimuth) domain. After focusing each track to a Single Look Complex (SLC) image

This article has been accepted for publication in a future issue of this journal, but has not been fully edited. Content may change prior to final publication. Citation information: DOI 10.1109/TGRS.2022.3171269, IEEE Transactions on Geoscience and Remote Sensing

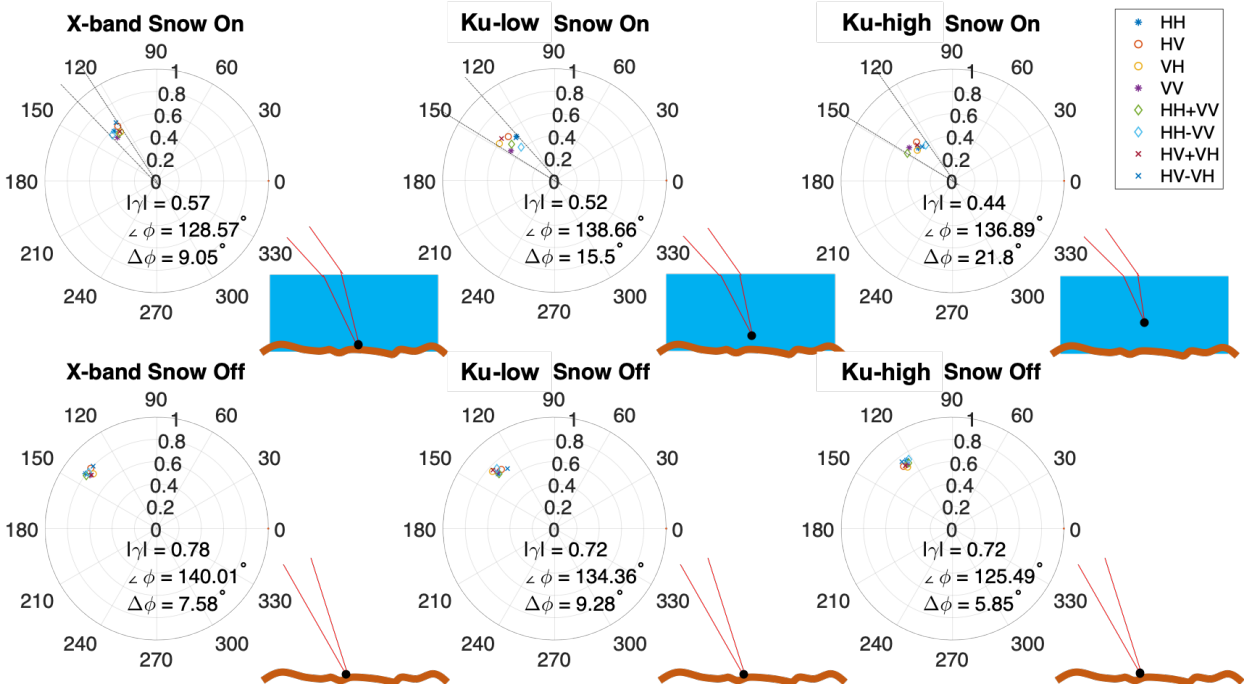

Fig. 6. Polarimetric InSAR analysis at three frequencies for both snow-on and snow-off scenarios. In each subplot, InSAR complex correlation of different polarizations are shown along with the average InSAR correlation magnitude $|\gamma|$, phase $\angle\phi$, and phase diversity (denoted by $\Delta\phi$), i.e., angle spanned by the black dotted lines. The same free-space interferometric vertical wavenumber $\tilde{\kappa_z} = 5.6$ rad/m is used for all subplots.

by using time domain back-projection algorithm, the two SLC images are then cross-correlated to form an interferogram by first flattening the phase with a flat constant-value DEM at the air-snow interface, and then followed by ensemble averaging of a ground area of 4 m (ground range) $\times$ 4 m (azimuth) at the antenna bore sight with a 2 $\times$ 2 multi-looking of the SLC's first. The spatial resolution of an X-band SLC is 0.42 m (ground range) $\times$ 0.37 m (azimuth), so a pixel spacing of 0.3 m is used in both directions, resulting in $\sim$ 100 independent samples. It took about 3 hours to complete a full tomographic scan (600 mm in both vertical and horizontal direction), where the maximum usable interferometric baseline in this work is only 100 mm that is one sixth of the full scan, indicating the maximum temporal baseline for the single-pass InSAR dataset is 0.5 hour. Therefore, the snow conditions are considered constant between the two SAR acquisitions.

The system was deployed on a ground based tower at the Fraser Experimental Forest (FEF) Headquarters, near Fraser, CO, USA (39.847°N, 105.912°W) from February 1 to April 30, 2017 and run continuously with some gaps for required hardware supports. In-situ measurements of snow depth and other snowpack properties (e.g. grain size, density and SWE) were performed every week for comparison with the remotely sensed data. The typical snow stratigraphy profiles (that are similar to the recommendation of [25]) of the density and grain size during that period can be found in Fig. 5, where the snow depth is 80 cm, average density is 225 kg/m^3, and grain size varies from 0.5 mm to 3 mm.

A network of soil moisture sensors, time-lapse cameras, acoustic depth sensors, laser depth sensor and meteorological instruments were installed next to the site to collect in-situ measurements of snow, weather, and soil conditions. As for modeling the snow-on ground surface location as well as the selection of the snow-free acquisition in both RVoG and FP models, soil moisture must be taken into account as the thaw/freeze state of soil can affect the snow-on/snow-free ground phase center location. For low frequencies such as L/C/X-band, the penetration depth can be neglected for wet soil, while for frozen soil, it can range from a few centimeters to tens of centimeters [26]–[28], which can bias the apparent snow-free InSAR phase center location and the modeled snow-on ground surface location (thus the inverted snow parameters). The snow-free acquisition can be obtained by deploying the radar over unfrozen soil either prior to the snow season or after snow melting. However, the inversion approaches need to be further investigated on correcting any possible InSAR phase center bias due to the snow-on ground location shift for frozen soil (e.g. snow-covered permafrost in high-latitude regions at L/C-band).

In our case, the radar was deployed after the snow accumulation (late December of 2016 through late January of 2017), so it is not possible to choose the snow-free acquisition prior to the snow season. Since snow gradually melted from mid-March to mid-April in 2017, we selected the data acquired on April 19 2017 as the snow-free acquisition, where the soil temperature at 5 cm depth is about 5-15$^\circ C$ with a soil moisture of 0.25 cm^3/cm^3 (thaw soil). During the snow-on period (February-March of 2017), the soil temperature at 5 cm is 0$^\circ C$ with a mean soil moisture of 0.1 cm^3/cm^3 (frozen soil). Here, the effect of ground location shift at X-band is considered less severe but does account for any resulting bias in the parameter inversion (as shown in Section III-C).

This article has been accepted for publication in a future issue of this journal, but has not been fully edited. Content may change prior to final publication. Citation information: DOI 10.1109/TGRS.2022.3171269, IEEE Transactions on Geoscience and Remote Sensing

A. Polarimetric InSAR analysis

The Polarimetric InSAR analysis of the three frequencies (X, Ku-low and Ku-high) are illustrated in Fig. 6 for both snow-on (20170201) and snow-off (20170419) scenarios, where the same free-space interferometric vertical wavenumber $\tilde{\kappa_z} = 5.6$ rad/m is used. From Fig. 6, the polarimetric phase diversity (maximum phase separation angle; denoted by $\Delta\phi$) is as small as 5°-10° for all three frequencies when snow-off. Focusing on the snow-on subplots, there is an increase of phase diversity and decrease of InSAR correlation magnitude as the frequency gets higher, which is consistent with the RVoG model prediction due to more polarization-dependent volume scattering at higher frequency. Comparing snow-on/off phase difference, we have $\delta\phi_c = -11.44°$ (X), $\delta\phi_c = 4.3°$ (Ku-low), and $\delta\phi_c = 11.4°$ (Ku-high). Using the FP model and substituting the in-situ measurement of snow depth of $d = 0.8$ m and snow density of 225 kg/m^3, we have the mean scattering center (averaging multi-polarizations) at $h = 0.8$ m (X), $h = 0.75$ m (Ku-low) and $h = 0.73$ m (Ku-high). This implies that the X-band scattering center is at the ground surface for dry snow, while higher frequencies (Ku-low and Ku-high) shift the scattering center further upwards due to more volume scattering.

As [12] reported, volume scattering at Ku-band can be neglected for the dry taiga snow. In our case, however, it can shift the phase center up by 5-7 cm. This can be explained as seen in Fig. 3, where Ku-band can be assumed to fully penetrate snow with smaller grain size (< 1.5 mm). When the grain size is big enough, e.g. the depth hoar layer with grain size of 1-3 mm in our in-situ stratigraphy profile (Fig. 5), the volume scattering effect cannot be ignored for Ku-band.

B. Ground-to-volume ratio analysis

As calculated by the QCA model (Fig. 3) and also shown by the experimental data in Fig. 6, the X-band radar signal has the potential to fully penetrate the dry snow to the underlying ground surface (i.e., there is minimal polarimetric dependence of the X-band InSAR phase center location), in what follows, we use X-band HH-pol InSAR data hereafter for the following validation of the single-pass InSAR model-based inversion approaches.

To investigate the conditions under which the X-band InSAR signal may or may not fully penetrate the snowpack, in this section, we use SAR Tomography to estimate GVR, although the InSAR approaches do not necessarily require the use of a TomoSAR system. The estimated GVR also serves as a parameter (i.e. m) for implementing/validating the RVoG model. The time series results of GVR and air temperature are illustrated in Fig. 7, where three different time periods of air-temperature-dependent snowpack conditions can be noticed. First, during the first week of February (Jan 30-Feb 6; see the closeup in the bottom panel of Fig. 7), the snowpack can be considered as fresh dry snow (as snow stopped accumulation in late January) and the temperature variation shows a clear diurnal cycle between -10°C to 5°C. From the GVR time series data and the two tomograms (in the top panel of Fig. 7), it can be seen that both volume scattering and GVR are generally high (> 3 dB) for cold weather (nighttime) and low (between 0 dB and 3 dB) for warm weather (daytime). Furthermore, there seems to be a consistent drop of GVR a few hours after the air temperature reaching the local maximum, and also an increase of GVR occurred a few hours after the air temperature dropping to the local minimum. Next, between Feb 07 and Feb 22, the air temperature strongly fluctuated with a big dynamic range, i.e., $\pm 10°C$, and the snowpack was expected to periodically turn wet. During that timeframe, we have two observations on Feb 9, where the GVR drops down to the minimum of -8 dB. For the third time period (after Feb 23), the air temperature dropped well below the freezing point (as low as -20°C), and the GVR observations (3 on Feb 27 and 1 on Mar 2) increased up to between -2 dB and 0 dB compared to the previous phase of wet snow. Although considered to be dry snow, the GVR during this time period is still lower than the first period of fresh dry snow condition, which can be explained by the change of the snowpack's metamorphic state after melting/refreezing (e.g. large and/or sticky particles formed causing bigger volume scattering) [29]. The third tomogram in the top panel of Fig. 7 confirms the existence of more volume scattering during this time period.

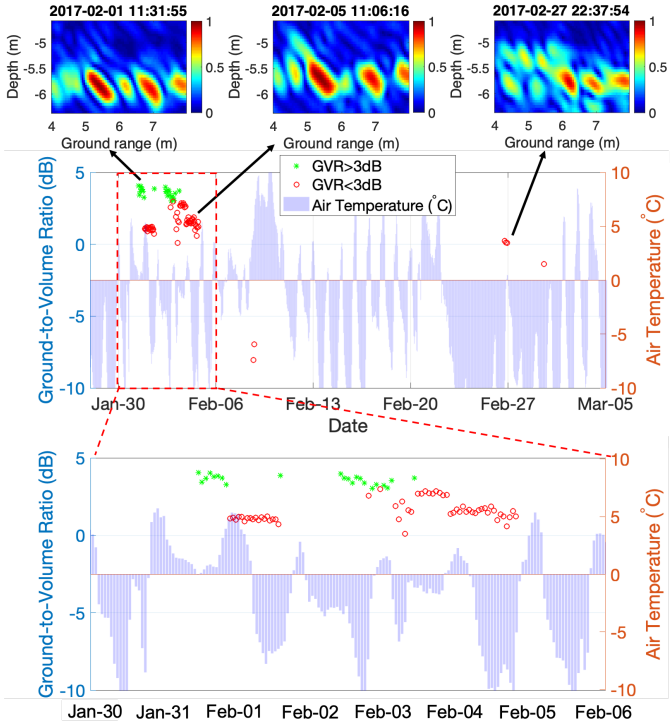

Fig. 7. Time series analysis of GVR estimates from SAR tomography, where the air temperature variation is overlaid. An empirical rule-of-thumb GVR threshold of 3 dB is used to distinguish snowpack conditions ("green" dots for GVR $>$ 3 dB, and "red" circles for GVR $<$ 3 dB). The tomograms (top panel) show the normalized coherence rather than absolute power level to facilitate discerning the existence of ground/volume scattering. The red dashed rectangle (in the middle panel) marks the first week of February with the closeup shown in the bottom panel.

Therefore, in this work, we empirically selected a rule-of-thumb GVR threshold of 3 dB to distinguish the snowpack conditions. When GVR $>$ 3 dB, the snowpack is likely

This article has been accepted for publication in a future issue of this journal, but has not been fully edited. Content may change prior to final publication. Citation information: DOI 10.1109/TGRS.2022.3171269, IEEE Transactions on Geoscience and Remote Sensing

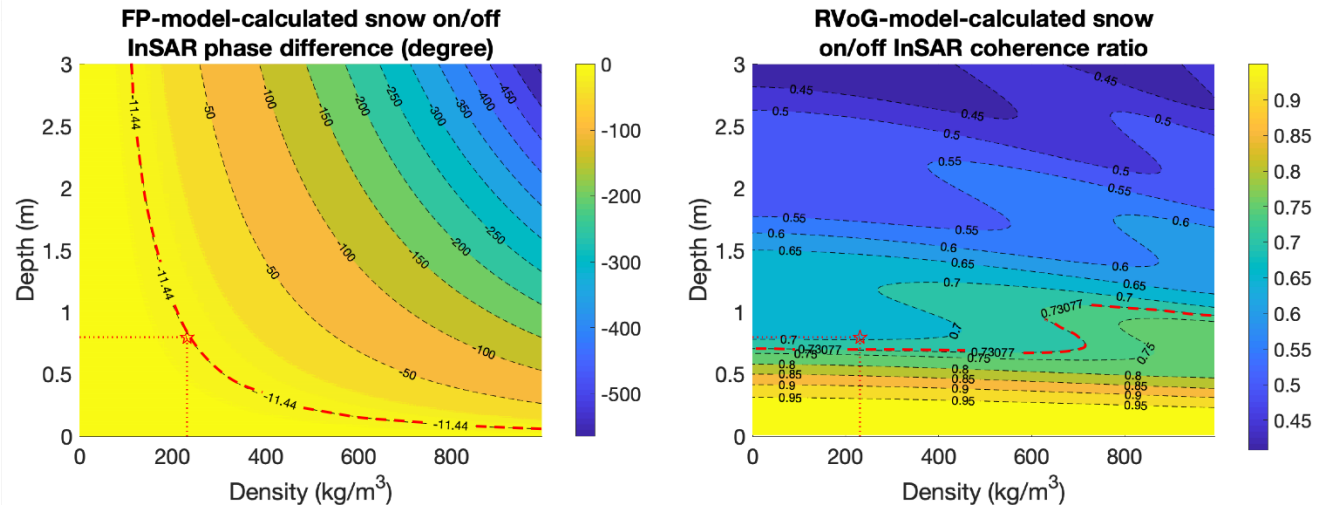

Fig. 8. The 2-D plot of FP-modeled snow on/off InSAR phase difference (left) and RVoG-modeled snow on/off InSAR coherence ratio (right) with contour lines for a wide range of snow conditions (as a function of snow depth and density). The red star marks the ground truth for the X-band HH-pol InSAR data collected on 20170201, and the red dashed curves show the contour lines of the measured quantities. The same free-space interferometric vertical wavenumber $\tilde{\kappa_z} = 5.6$ rad/m is used as in Fig. 6.

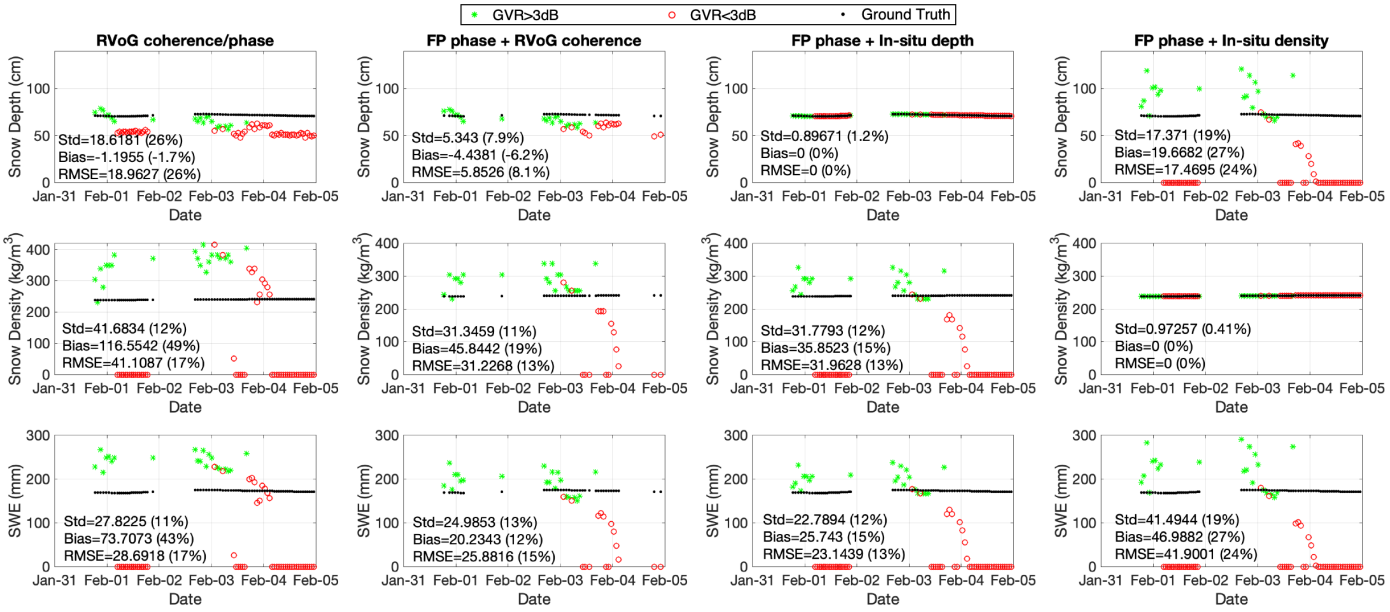

Fig. 9. Snow inversion results using the single-pass InSAR approaches with scattering model inversion. Each row corresponds to one snow parameter (depth, density and SWE), while each column corresponds to one modeled inversion approach: 1) RVoG-modeled InSAR coherence and phase, 2) FP-modeled phase and RVoG-modeled coherence, 3) FP-modeled phase and in-situ depth, and 4) FP-modeled phase and in-situ density. Results are shown for both cases of GVR > 3 dB ("green" dots) and GVR < 3 dB ("red" circles) which are defined the same as in Fig. 7. The same free-space interferometric vertical wavenumber $\tilde{\kappa_z} = 5.6$ rad/m is used.

dominated by fresh dry snow, which has minimal volume scattering thus easily justifying the zero extinction assumption at low frequencies. When GVR $<$ 3 dB, the snowpack condition is complicated (e.g. dry snow that diurnally turns a bit wet, extremely wet snow after melting, and refrozen snow after periods of thaw/refreezing that changes the metamorphic state) so that the single-pass InSAR approaches developed in this work may or may not work depending on the actual snowpack condition. As shown in Fig. 7 and also in the following validations, we discern these two cases using two different types of markers (i.e., "green" dots for GVR $>$ 3 dB, and "red" circles for GVR $<$ 3 dB). Note in Section III-D, non-trivial values of k_e will be selected through the RVoG forward model analysis to quantitatively characterize the GVR $<$ 3 dB case.

C. Snow parameter inversion

Using the full snow InSAR dataset, we next validate the two InSAR scattering models: RVoG and FP. Since the FP model only provides one InSAR phase measurement (with

This article has been accepted for publication in a future issue of this journal, but has not been fully edited. Content may change prior to final publication. Citation information: DOI 10.1109/TGRS.2022.3171269, IEEE Transactions on Geoscience and Remote Sensing

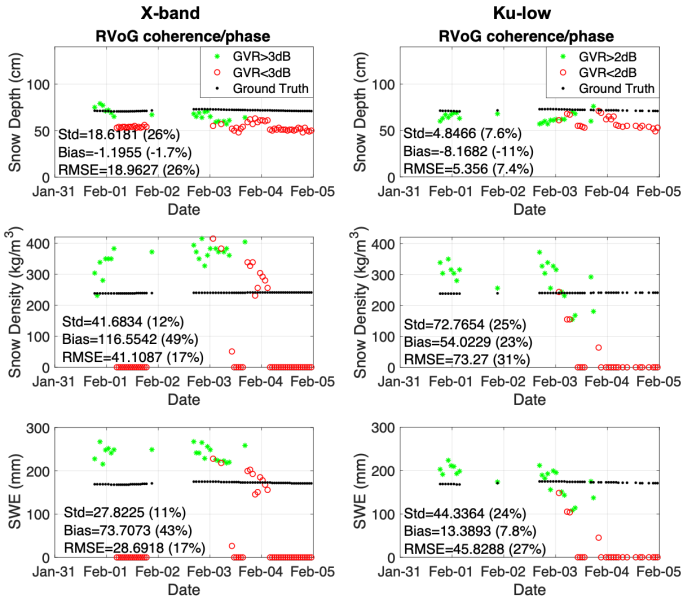

Fig. 10. RVoG model-based snow inversion comparison between X-band (left column) and Ku-low (right column). The X-band result (left column) here is the same as the first column in Fig. 9. Note the Ku-low rule-of-thumb GVR threshold is empirically selected as 2 dB versus the 3 dB GVR threshold at X-band.

two unknowns), we have to incorporate another dimension of measurement or in-situ data to further constrain snow depth and density.

In Fig. 8, we illustrate the FP-modeled snow on/off InSAR phase difference and the RVoG-modeled snow on/off InSAR coherence ratio for the X-band HH-pol InSAR dataset collected on 20170201, as used in Fig. 6 (Section III-A), where a wide range of candidate snow conditions are plotted. It is known that the density of terrestrial dry snow is usually smaller than 500 kg/m^3, while firn in glacierized regions could reach up to 800 kg/m^3 [30]. It can be noticed from Fig. 8 that, the contour lines of the FP modeled InSAR phase provides a set of hyperbola-like functions of snow depth and density, which have different inversion/sensitivity behavior at each side of the vertex point of the hyperbola (more obvious at the lower left corner of the 2-D plot). For example, to the left of the vertex point (where the ground truth red star is located; dominated by terrestrial dry snow with low density), density can be determined confidently given a measured/in-situ depth, however, given a measured/in-situ density value, depth may have noticeable bias and uncertainty due to decreased measurement sensitivity in that region. The opposite can be inferred when the ground truth moves to the right of the vertex point (mostly dense/shallow terrestrial dry snow and firn). This implies that for the dry snow conditions over our test site, the FP-modeled InSAR phase combined with in-situ depth has much better inversion performance than the FP-modeled InSAR phase combined with in-situ density. Furthermore, the contour lines of the RVoG-modeled InSAR coherence almost constrain the snow depth values rather than density (more obvious at small depths and become ambiguous for large depths), which also implies that the FP-modeled phase combined with RVoG-modeled coherence should provide an inversion performance as good as the FP-modeled phase combined with in-situ depth. This analysis is verified with the following inversion results. Also as shown in Fig. 8, the contour lines of the measured quantities (red dashed curves) almost passed through the ground truth (red star).

Next, we consider three scenarios for incorporating an extra measurement or in-situ data to combine with the FP-modeled InSAR phase: 1) using the RVoG-modeled InSAR coherence, 2) using the in-situ depth, and 3) using the in-situ density. The snow inversion results for all three scenarios along with the RVoG model results are illustrated in Fig. 9. First of all, only the results during the first week of February are demonstrated, since observations acquired during the other time periods most likely failed on the model inversion, which is due to the invalid zero extinction assumption for those time periods (as discussed in Section III-B and will be treated separately in Section III-D). Further, part of the GVR < 3 dB case ("red" circles) also has good inverted results, which corresponds to the wetness of the snowpack during the diurnal variation. As mentioned in Section III-B, when GVR > 3 dB, the accuracy of the model inversion is more guaranteed, while for GVR < 3 dB, snowpack condition tends to become more complicated and the validity/performance of the model inversion depends the actual snowpack condition (that also correlates with the GVR as shown in Fig. 7).

From Fig. 9, the FP-modeled phase combined with the RVoG-modeled coherence or the in-situ depth (i.e., the last row of the second and third columns) provide the best and comparable SWE inversion results (as well as depth/density) with Root Mean Square Error (RMSE) of 23-26 mm (13-15%) and bias of 20-26 mm (12-15%), which is consistent with the above contour-line analysis (Fig. 8). The RVoG-modeled results are worse with 28.7 mm (17%) RMSE and 73.7 mm (43%) bias which could be due to the model complexity and the uncertainty in estimating the model parameters such as m and k_e (Section II-A) and thus serves as the worst-case scenario. Note the snow-on ground location shift due to frozen underlying soil may account for the inversion bias here. Similarly, the results by using FP-modeled phase combined with in-situ density are moderately worse with 42 mm (24%) RMSE and 47 mm (27%) bias, which is due to the decreased sensitivity of the FP-modeled phase in measuring depth to the left of the hyperbola vertex point, as explained above in interpreting Fig. 8. This analysis justifies the potential of using the FP model as a single constraint of snow depth and density, which can be used in combination with RVoG-modeled coherence or an extra depth measurement (if ground truth is located to the left of the vertex point of the hyperbolic contour lines), and with an extra density measurement (if ground truth is located to the right of the vertex point).

In Fig. 10, we also compare the performance of the RVoG model inversion at X-band and Ku-low, where the Ku-low rule-of-thumb GVR threshold is empirically selected as 2 dB versus the 3 dB GVR threshold at X-band. Compared to the X-band RVoG inverted results, the Ku-low results provide generally comparable inversion performance, with higher RMSE (27%)

This article has been accepted for publication in a future issue of this journal, but has not been fully edited. Content may change prior to final publication. Citation information: DOI 10.1109/TGRS.2022.3171269, IEEE Transactions on Geoscience and Remote Sensing

but smaller bias (7.8%). As discussed in the QCA-based extinction analysis (Fig. 3), the Ku-band (both Ku-low and Ku-high) signals tends to violate the zero extinction assumption as the snow grain size gets larger, thus not recommended to use in practice as opposed to other low frequencies (L/C/X-band). Also, as discussed in Section III-A, the Ku-band snow-on InSAR phase center is not located on the ground surface, thus prohibiting the use of FP model for the Ku-band inversion.

The dependence of the inversion performance on interferometric baseline (or equivalently $\tilde{\kappa_z}$) is shown in Fig. 11. It can be seen that the depth inversion has an optimal baseline region of 40-100 mm ($\tilde{\kappa_z}$ of 2-6 rad/m) that is close to a tenth of the snow depth of 80 cm, while the density inversion has a larger fluctuating uncertainty at the lower end and converges to the true value as baseline reaches 80 mm ($\tilde{\kappa_z}$ of 4.5 rad/m). Therefore, SWE inversion (by multiplying depth and density) is relatively accurate over the baseline range of 60-100 mm ($\tilde{\kappa_z}$ of 3-6 rad/m), which is also close to a tenth of the snow depth being measured.

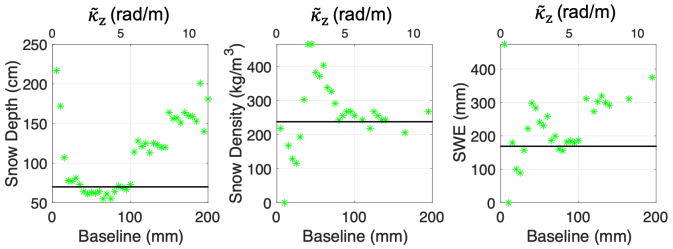

Fig. 11. Interferometric baseline dependence of the inversion performance at X-band on all three snow parameters (depth, density and SWE), where both the baseline (bottom scale) and $\tilde{\kappa_z}$ (top scale) are shown. Here, the inversion approach of using FP-modeled phase and RVoG-modeled coherence (second column of Fig. 9) is used for the dataset on 20170201, where the ground truth data are shown as black solid lines.

Since the dry snow conditions of our test site are very limited (with almost constant values of depth and density), we next run simulations to examine the inversion performance and error propagation for a wide range of dry snow conditions in Fig. 12, i.e. snow depth of 0-3 m, density of 0-500 kg/m^3, and SWE of 0-1.5 m. For the inversion approach, we use the FP-modeled InSAR phase combined with the RVoG-modeled InSAR coherence. Regarding each point in a 2-D subplot, 100 Monte-Carlo simulations were performed assuming a measurement uncertainty of 0.2 for InSAR coherence and 200 millidegrees for InSAR phase.

First of all, it can be noticed that all subplots have various degrees of finge-like pattern, which is due to the use of ambiguous RVoG-modeled InSAR coherence as illustrated in Fig. 8 for large depths. It can be seen that both the inversion bias and uncertainry of all three snow parameters are negligible for dry snow with small depth values (< 0.8 m). The depth inversion bias increases up to 0.4 m for snow depths of 2-2.5 m (17%), where the depth inversion uncertainty reaches 0.35 m (16%). However, the density inversion bias reaches up to 300 kg/m^3 for deep dry snow (e.g. depth of 1.5-3 m) with the uncertainty being up to 400 kg/m^3. This large density inversion bias/uncertainty at the finge-like pattern is also because of the ambiguous measurement of RVoG-modeled InSAR coherence (right subplot of Fig. 8; excluding the small-depth regions), which could be further mitigated a lot if using in-situ or other depth measurements without ambiguity. By multiplying depth and density, the SWE inversion bias and uncertainty also resemble the pattern of both depth and density, where both the inversion bias and uncertainty are $\ll 10$ cm for depth of 0-0.8 m, around 50 cm for depth of 0.8-1.5 m and around 100 cm for depth of 1.5-3 m.

D. RVoG Forward Model Analysis ($k_e \neq 0$)

As discussed in Section III-B, when GVR < 3 dB, snowpack condition becomes complicated (e.g. dry snow that diurnally turns a bit wet, extremely wet snow after melting, and refrozen snow after periods of thaw/refreezing that changes the metamorphic state), which imposes various degrees of the extinction effect, thus violating the zero extinction assumption (Section II-A). As seen from Section II-A, besides snow parameters (depth and density), the RVoG model has two extra unknowns: GVR m and extinction coefficient k_e. If $k_e \neq 0$, neither snow parameters nor k_e can be uniquely determined from a single InSAR observation. Therefore, in this section, we perform an RVoG forward model analysis by fitting the in-situ measured ground truth snow parameters to the RVoG model without making zero extinction assumption, which in turn determines the single fitting parameter k_e. The time series of the determined k_e is illustrated in the bottom panel of Fig. 13. Next, through using this fitted k_e estimate, we can then verify the RVoG model accuracy by inverting for snow depth, density and SWE. These inverted snow parameters are shown in the top three panels of Fig. 13.

From Fig. 13, first of all, it can be seen that almost the entire time series dataset (corresponding to the full GVR time series Fig. 7) can be used for RVoG model inversion as opposed to the first week of February in Fig. 9. In particular, several GVR < 3 dB observations have been successfully used to retrieve the snow parameters to a plausible accuracy, including the wet snow and refrozen snow time periods as identified in Section III-B. Focusing on the forward model determined k_e estimates, the first week of February (dominated by fresh dry snow) can be primarily characterized by zero extinction $k_e = 0$. During the second time period (wet snow on Feb 9), the determined extinction reaches up to 10 dB/m. Regarding the third time period (refrozen snow on Feb 27 and Mar 2), the extinction is estimated to be 1 dB/m and 5.3 dB/m, respectively. This result explains why the above-developed model inversion approaches with zero extinction assumption (or equivalently $k_e \leq 0.5$ dB/m) failed to retrieve snow parameters for the wet and refrozen snow cases that both have $k_e \geq 1$ dB/m. Given that the X-band k_e of refrozen snow is only moderately bigger (1-5 dB/m), using the above model inversion approaches at lower frequencies (e.g. L/C-band) has the potential to retrieve the parameters of refrozen snow.

Regarding modeling such big k_e, the QCA dense medium model is not sufficient, as it only allows the use of unrealistically big grain sizes to realize such big k_e (see the trend in Fig. 3). In contrast, it can be achieved by incorporating the stickiness to QCA for characterizing the particle aggregation

This article has been accepted for publication in a future issue of this journal, but has not been fully edited. Content may change prior to final publication. Citation information: DOI 10.1109/TGRS.2022.3171269, IEEE Transactions on Geoscience and Remote Sensing

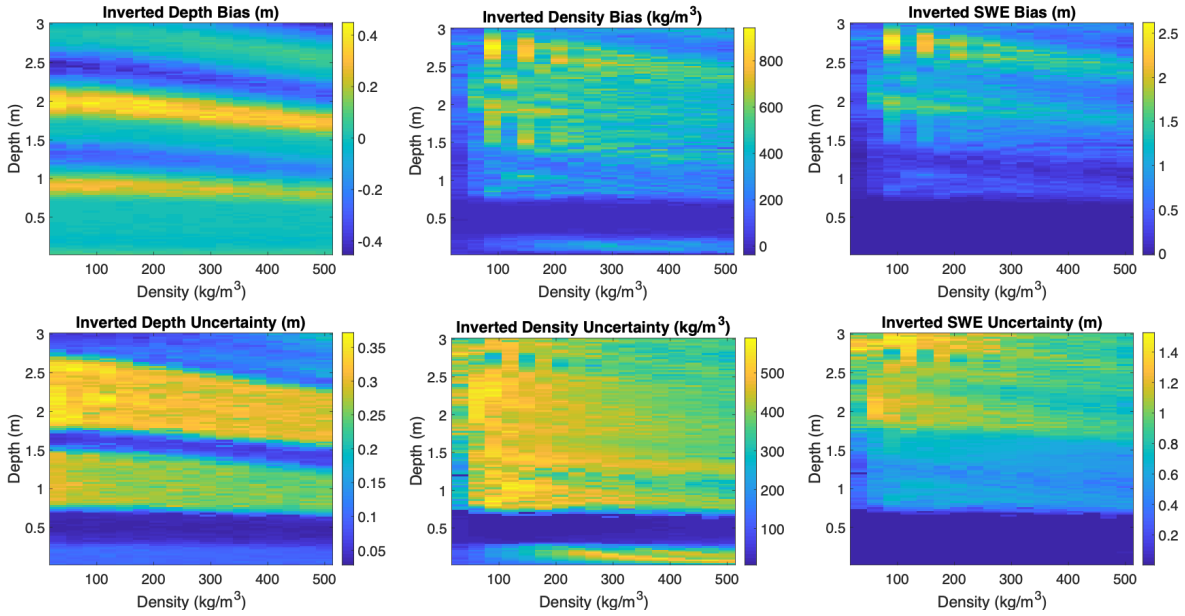

Fig. 12. Simulated 2-D inversion bias and uncertainty for each of the three snow parameters and a wide range of dry snow conditions. Each column corresponds to a snow parameter (depth, density and SWE), and each row represents inversion bias and/or uncertainty. For each point in a 2-D subplot, 100 Monte-Carlo simulations were performed to get the bias/uncertainty metric, where a measurement uncertainty of 0.2 for InSAR coherence and 200 millidegrees for InSAR phase are assumed. Only the FP-modeled InSAR phase combined with the RVoG-modeled InSAR coherence is tested here with the same free-space interferometric vertical wavenumber $\tilde{\kappa_z} = 5.6$ rad/m.

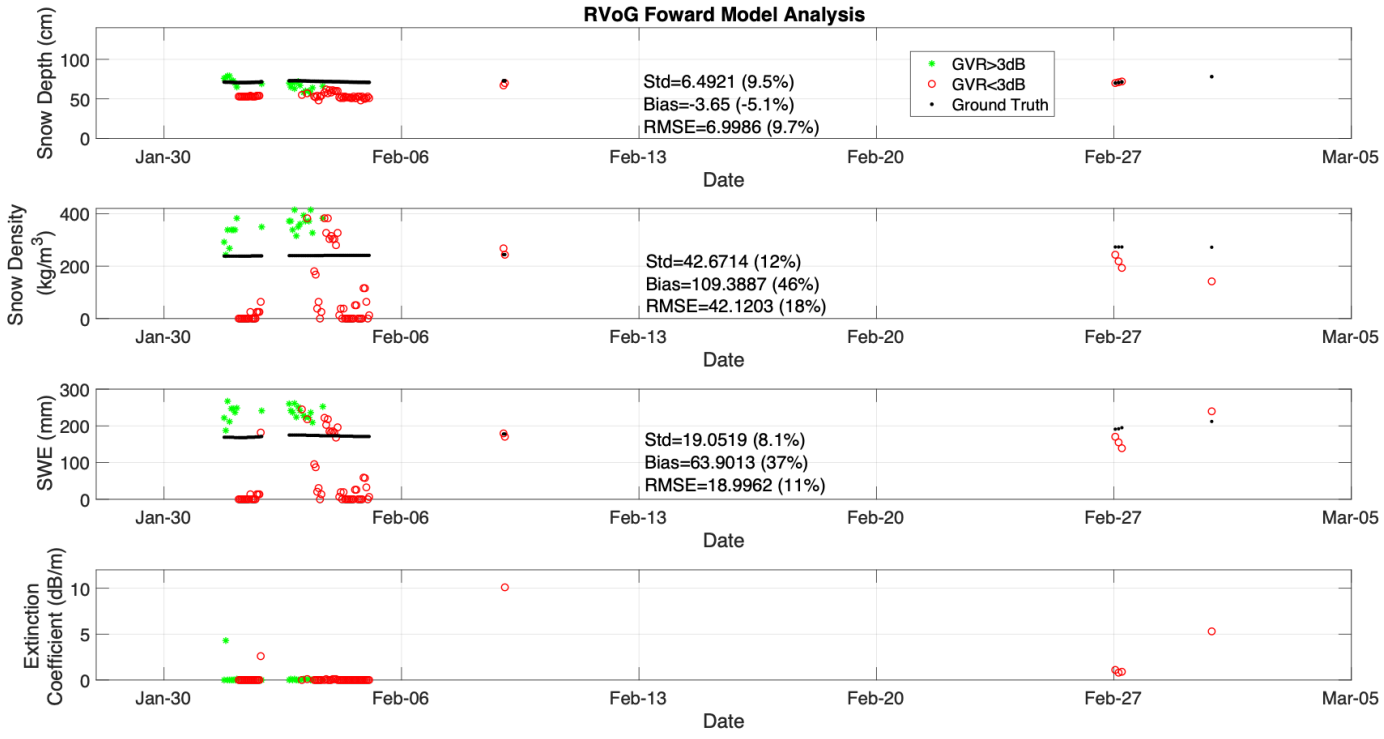

Fig. 13. RVoG forward model analysis: the bottom panel shows the RVoG forward model-determined extinction coefficient k_e by fitting the in-situ measured snow parameters (depth and density) to the RVoG model without zero extinction assumption, and the top three panels demonstrate the RVoG inverted results of snow depth, density and SWE, respectively, using the RVoG forward model-determined k_e. Results are shown for both cases of GVR > 3 dB ("green" dots) and GVR < 3 dB ("red" circles) which are defined the same as in Fig. 7. The same free-space interferometric vertical wavenumber $\tilde{\kappa_z} = 5.6$ rad/m is used.

as modeled by the QMS (QCA Mie scattering of Sticky spheres) dense medium model [31], as well as by using the Bi-continuous dense medium model for better representing the snow microstructures with irregular shape and aggregation of ice particle [32].

IV. Discussion and Conclusions

A. Summary

In this paper, we have shown the potential of retrieving dry snow parameters by using single-pass InSAR approaches based on inversion of scattering models: 1) the dense-medium RVoG model, and 2) the simple variant (FP model). In order to invert the dense medium RVoG model that has two extra unknowns (GVR m and extinction coefficient k_e), we brought forward the zero extinction assumption (or equivalently $k_e \leq 0.5$ dB/m) for low frequencies (L/C/X-band), and validated it using the QCA dense medium model. The model parameter of GVR, m, is inferred from the tomogram in this work. Similar to the repeat-pass InSAR approaches, the FP model assumes the radar signal can fully penetrate the snow volume at low frequencies (L/C/X-band), and thus the apparent InSAR phase provides a relationship constraining snow depth and density, which was further supplemented by an extra observation: 1) RVoG-modeled InSAR coherence, 2) in-situ depth and 3) in-situ density.

With a tower-based TomoSAR system, a multi-frequency polarimetric InSAR analysis and a GVR time series analysis were performed to investigate the polarization/frequency-dependence of InSAR observations, as well as to distinguish the temporal variation of snowpack conditions. It was found that X-band radar signals can fully penetrate fresh dry snow with the InSAR phase center located at the underlying ground surface and with minimal polarimetric dependence. Also, the GVR inversely changes with the air temperature for normal diurnal variation, and rapidly drops for wet and/or refrozen snow, where a rule-of-thumb threshold of 3 dB was used to identify the different snow conditions at our test site. In future work, comprehensive experiments and modeling of the various snowpack conditions that cause the GVR drop (thus k_e increase) are needed to analyze the correlation between GVR (also k_e) and the relevant environmental factors (e.g. air temperature), so that a physical GVR threshold (and ranges of k_e) may be properly selected for distinguishing the snow conditions.

Using X-band HH-pol InSAR data over the fresh dry snow, the FP-modeled single-pass InSAR phase along with RVoG-modeled coherence or in-situ depth is capable of measuring SWE with 23-26 mm (13-15%) RMSE and 20-26 mm (12-15%) bias. Unfortunately, the snow sample dataset in this work is very limited, i.e. almost constant values for the whole snow season of year 2017. Therefore, by using the 2-D contour lines of the measured quantities as well as Monte-Carlo simulations for a wide range of snow conditions, we also analyzed the sensitivity and error propagation of the single-pass InSAR phase and coherence in measuring dry snow depth/density. It was found that for dry snow conditions to the left of the hyperbola vertex point of the contour lines (mostly terrestrial dry snow with low density), InSAR phase has better sensitivity of density rather than depth (thus can be supplemented by in-situ or other depth measurements), while to the right of the vertex point (mostly dense/shallow terrestrial dry snow and firn), better sensitivity to depth rather than density can be achieved, which can be supplemented by in-situ or other density measurements. The InSAR coherence accurately constrains the snow depth at small depth values (< 0.8 m) but becomes ambiguous for large depths. Therefore, over such snow conditions with large depths, the InSAR coherence needs to be replaced with in-situ or other type of depth measurements; otherwise, large inversion bias/uncertainty will be resulted for both density and SWE. By analyzing the interferometric baseline (or vertical wavenumber) dependence of the model inversion performance, an optimal perpendicular baseline was found to be on the order of a tenth of snow depth.

B. Limitations and Future Work

Note this paper is focused on the concept development of the single-pass InSAR approach along with its validation using a ground-based TomoSAR/InSAR system. Although the extension of this approach for airborne and spaceborne SAR/InSAR platforms is highly desired, several limitations with future improvements must be further investigated to reliably generalize or extend this approach.

From the baseline/$\tilde{\kappa_z}$-dependence analysis (Fig. 11), it was shown that an optimal baseline range of 60-100 mm ($\tilde{\kappa_z}$ of 3-6 rad/m) is needed for SWE retrieval, and 40-100 mm ($\tilde{\kappa_z}$ of 2-6 rad/m) for snow depth retrieval. This requirement partially agrees with [23] on using bigger $\tilde{\kappa_z}$ such as 1-2 rad/m for snow depth retrieval. However, realizing such big $\tilde{\kappa_z}$ or interferometric baseline in space is not trivial, which is further limited by the critical baseline. The critical baseline depends on the center frequency and bandwidth of the radar system, the slant-range distance from radar to the target, as well as the incidence angle. The critical baseline of our ground-based TomoSAR system is 368 mm at X-band and 262 mm at Ku-low, so the optimal baseline of 40-100 mm for snow retrieval is well below it. However, for a spaceborne low-frequency (L/C/X-band) InSAR system, it is recommended to design the radar system with adequate bandwidth, as well as to use a viewing geometry with big orbital height and look angle.

When applying the approaches to sloped terrain (e.g., high topographic relief), $\tilde{\kappa_z}$ and κ_z need to be calculated with the local incidence and/or refraction angle on a pixel-by-pixel basis. Further, the underlying sloped topography needs to be removed during the flattening of InSAR phase.

As implied from the X-band inversion analysis, the existing spaceborne X-band single-pass InSAR system, TanDEM-X mission, can be used for testing the inversion approaches developed in this paper on fresh dry snow retrieval when using bigger $\tilde{\kappa_z}$, however, it may not work well for refrozen snow. For retrieving both fresh and refrozen snow parameters, a lower frequency (L/C-band) spaceborne single-pass InSAR system would be desirable, e.g. TanDEM-L. Modeling snow conditions with big k_e for refrozen snow can also be refined by incorporating the stickiness (QMS model) and discretized snow miscrostructure (Bi-continuous model).

As for the inversion approaches, the FP model is simple and requires less model parameters (thus less model uncertainty in the inversion), which is recommended to use in combination with other types of in-situ and remote sensing measurements of snow depth/density (e.g. SAR backscatter at L/C/X-band [22],

[33]). As for the use of the dense medium RVoG model [20], due to the lack of polarization diversity and the dominated ground scattering in the InSAR observables, the extra model parameters (extinction coefficient k_e and GVR m) cannot be isolated or uniquely determined from the measurement of existing spaceborne interferometric (and polarimetric) SAR systems. Other modeling or remote sensing methods need to be developed for independently retrieving k_e and m from space. Alternatively, as demonstrated in this work, the dense medium RVoG model together with a ground-based TomoSAR system serves as a useful tool for algorithm development and validation, which sheds light on applying the developed snow retrieval algorithms to airborne/spaceborne InSAR systems.

Regarding the application of the inversion approaches to the snow-covered permafrost in high-latitude regions using low frequencies (L/C-band), the non-trivial penetration depth into the frozen soil can bias the snow-on ground surface location (thus the inverted snow parameters) by a few centimeters to tens of centimeters, which needs further investigation in future work for correcting any possible InSAR phase center bias.

Due to the scarcity of the experimental dataset used in this work (almost constant values during the snow season at the current test site), it is only validated for one snow condition: snow depth of 0.8 m, density of 225 kg/m^3 and SWE of 0.2 m. Although we demonstrated the validation of it over a wide range of snow conditions through simulation (Fig. 12), it is important to validate this approach over other types of snow conditions by employing ground-based InSAR/TomoSAR systems, as well as exploiting the available airborne/spaceborne single-pass InSAR dataset.

Indeed, the above limitations/improvements need to be further investigated in order to better assess the capability of generalizing or extending this approach. By noting and addressing the above limitations/improvements properly, the model-based single-pass InSAR inversion approaches are potentially useful and thus need to be validated in future work for large-scale dry snow retrieval with various snow conditions using ground-based/airborne/spaceborne low-frequency (L/C/X-band) single-pass InSAR observations.

ACKNOWLEDGMENT

We would like to acknowledge Torry Akins of Remote Sensing Solutions Inc., and Rashmi Shah of JPL for their guidance and support.

REFERENCES

[1] T. P. Barnett, J. C. Adam, and D. P. Lettenmaier, "Potential impacts of a warming climate on water availability in snow-dominated regions," *Nature*, vol. 438, no. 7066, pp. 303–309, 2005.

[2] M. Sturm, M. A. Goldstein, and C. Parr, "Water and life from snow: A trillion dollar science question," *Water Resources Research*, vol. 53, no. 5, pp. 3534–3544, 2017.

[3] I. T. Stewart, "Changes in snowpack and snowmelt runoff for key mountain regions," *Hydrological Processes: An International Journal*, vol. 23, no. 1, pp. 78–94, 2009.

[4] J. Shi, C. Xiong, and L. Jiang, "Review of snow water equivalent microwave remote sensing," *Science China Earth Sciences*, vol. 59, no. 4, pp. 731–745, 2016.

[5] Y.-L. S. Tsai, A. Dietz, N. Oppelt, and C. Kuenzer, "Remote sensing of snow cover using spaceborne sar: A review," *Remote Sensing*, vol. 11, no. 12, p. 1456, 2019.

[6] P. A. Rosen, S. Hensley, I. R. Joughin, F. K. Li, S. N. Madsen, E. Rodriguez, and R. M. Goldstein, "Synthetic aperture radar interferometry," *Proceedings of the IEEE*, vol. 88, no. 3, pp. 333–382, 2000.

[7] K. P. Papathanassiou and S. R. Cloude, "Single-baseline polarimetric sar interferometry," *IEEE Transactions on Geoscience and Remote Sensing*, vol. 39, no. 11, pp. 2352–2363, 2001.

[8] T. Guneriussen, K. A. Hogda, H. Johnsen, and I. Lauknes, "Insar for estimation of changes in snow water equivalent of dry snow," *IEEE Transactions on Geoscience and Remote Sensing*, vol. 39, no. 10, pp. 2101–2108, 2001.

[9] H. Rott, T. Nagler, and R. Scheiber, "Snow mass retrieval by means of sar interferometry," in *3rd FRINGE Workshop, European Space Agency, Earth Observation*. Citeseer, 2003, pp. 1–6.

[10] G. Engen, T. Guneriussen, and Y. Overrein, "Delta-k interferometric sar technique for snow water equivalent (swe) retrieval," *IEEE Geoscience and remote sensing letters*, vol. 1, no. 2, pp. 57–61, 2004.

[11] E. J. Deeb, H.-P. Marshall, R. R. Forster, C. E. Jones, C. A. Hiemstra, and P. R. Siqueira, "Supporting nasa snowex remote sensing strategies and requirements for l-band interferometric snow depth and snow water equivalent estimation," in *2017 IEEE International Geoscience and Remote Sensing Symposium (IGARSS)*. IEEE, 2017, pp. 1395–1396.

[12] S. Leinss, A. Wiesmann, J. Lemmetyinen, and I. Hajnsek, "Snow water equivalent of dry snow measured by differential interferometry," *IEEE Journal of Selected Topics in Applied Earth Observations and Remote Sensing*, vol. 8, no. 8, pp. 3773–3790, 2015.

[13] S. Leinss, J. Lemmetyinen, A. Wiesmann, and I. Hajnsek, "Interferometric and polarimetric methods to determine swe, fresh snow depth and the anisotropy of dry snow," in *2015 IEEE International Geoscience and Remote Sensing Symposium (IGARSS)*. IEEE, 2015, pp. 4029–1032.

[14] E. J. Deeb, R. R. Forster, and D. L. Kane, "Monitoring snowpack evolution using interferometric synthetic aperture radar on the north slope of alaska, usa," *International journal of remote sensing*, vol. 32, no. 14, pp. 3985–4003, 2011.

[15] S. Leinss, O. Antropov, J. Vehviläinen, J. Lemmetyinen, I. Hajnsek, and J. Praks, "Wet snow depth from tandem-x single-pass insar dem differencing," in *IGARSS 2018-2018 IEEE International Geoscience and Remote Sensing Symposium*. IEEE, 2018, pp. 8500–8503.

[16] H. Rott, S. Scheiblauer, J. Wuite, L. Krieger, D. Floricioiu, P. Rizzoli, L. Libert, and T. Nagler, "Penetration of interferometric radar signals in antarctic snow," *The Cryosphere*, vol. 15, no. 9, pp. 4399–4419, 2021.

[17] R. N. Treuhaft and P. R. Siqueira, "Vertical structure of vegetated land surfaces from interferometric and polarimetric radar," *Radio Science*, vol. 35, no. 1, pp. 141–177, 2000.

[18] E. W. Hoen and H. A. Zebker, "Penetration depths inferred from interferometric volume decorrelation observed over the greenland ice sheet," *IEEE Transactions on Geoscience and Remote Sensing*, vol. 38, no. 6, pp. 2571–2583, 2000.

[19] J. Dall, "Insar elevation bias caused by penetration into uniform volumes," *IEEE Transactions on Geoscience and remote sensing*, vol. 45, no. 7, pp. 2319–2324, 2007.

[20] Y. Lei, P. Siqueira, and R. Treuhaft, "A dense medium electromagnetic scattering model for the insar correlation of snow," *Radio Science*, vol. 51, no. 5, pp. 461–480, 2016.

[21] Z. Li, Z. Li, B. Tian, and J. Zhou, "An insar scattering model for multi-layer snow based on quasi-crystalline approximation (qca) theory." *Science China Earth Sciences*, vol. 61, no. 8, 2018.

[22] J. Shi and J. Dozier, "Estimation of snow water equivalence using sir-c/x-sar. i. inferring snow density and subsurface properties," *IEEE Transactions on geoscience and remote sensing*, vol. 38, no. 6, pp. 2465–2474, 2000.

[23] S. Leinss and I. Hajnsek, "Opportunities of snow property extraction based on single and multi pass sar interferometry: Tandem-x," in *2012 IEEE International Geoscience and Remote Sensing Symposium*. IEEE, 2012, pp. 146–149.

[24] X. Xu, C. A. Baldi, J.-W. De Bleser, Y. Lei, S. Yueh, and D. Esteban-Fernandez, "Multi-frequency tomography radar observations of snow stratigraphy at fraser during snowex," in *IGARSS 2018-2018 IEEE International Geoscience and Remote Sensing Symposium*. IEEE, 2018, pp. 6269–6272.

[25] C. Fierz, R. L. Armstrong, Y. Durand, P. Etchevers, E. Greene, D. M. McClung, K. Nishimura, P. K. Satyawali, and S. A. Sokratov, "The international classification for seasonal snow on the ground," 2009.

[26] J. Du, J. S. Kimball, and M. Moghaddam, "Theoretical modeling and analysis of l-and p-band radar backscatter sensitivity to soil active layer dielectric variations," *Remote Sensing*, vol. 7, no. 7, pp. 9450–9472, 2015.

[27] H. Bergstedt, S. Zwieback, A. Bartsch, and M. Leibman, "Dependence of c-band backscatter on ground temperature, air temperature and snow depth in arctic permafrost regions," *Remote Sensing*, vol. 10, no. 1, p. 142, 2018.

[28] S. Leinss, G. Parrella, and I. Hajnsek, "Snow height determination by polarimetric phase differences in x-band sar data," *IEEE Journal of Selected Topics in Applied Earth Observations and Remote Sensing*, vol. 7, no. 9, pp. 3794–3810, 2014.

[29] B. Reber, C. Mätzler, and E. Schanda, "Microwave signatures of snow crusts modelling and measurements," *International Journal of Remote Sensing*, vol. 8, no. 11, pp. 1649–1665, 1987.

[30] K. J. Bormann, S. Westra, J. P. Evans, and M. F. McCabe, "Spatial and temporal variability in seasonal snow density," *Journal of Hydrology*, vol. 484, pp. 63–73, 2013.

[31] L. Tsang, J. Pan, D. Liang, Z. Li, D. W. Cline, and Y. Tan, "Modeling active microwave remote sensing of snow using dense media radiative transfer (dmrt) theory with multiple-scattering effects," *IEEE Transactions on Geoscience and Remote Sensing*, vol. 45, no. 4, pp. 990–1004, 2007.

[32] X. Xu, L. Tsang, and S. Yueh, "Electromagnetic models of co/cross polarization of bicontinuous/dmrt in radar remote sensing of terrestrial snow at x-and ku-band for coreh2o and sclp applications," *IEEE Journal of Selected Topics in Applied Earth Observations and Remote Sensing*, vol. 5, no. 3, pp. 1024–1032, 2012.

[33] J. Shi and J. Dozier, "Estimation of snow water equivalence using sir-c/x-sar, part ii: Inferring snow depth and particle size," *IEEE Transactions on Geoscience and Remote sensing*, vol. 38, no. 6, pp. 2475–2488, 2000.